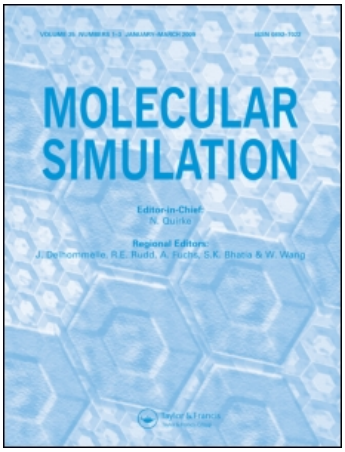

Molecular Simulation

Publication details, including instructions for authors and subscription information:
http://www.informaworld.com/smpp/title~content=t713644482

Structural and spectroscopic study of 3,6-dibutanoic-1,2,4,5-tetroxane

J. M. Romero[a]; M. I. Profeta[a]; N. L. Jorge[a]; M. E. Gómez-Vara[a]; E. A. Castro[b]; A. H. Jubert[c]
[a] Área de Fisicoquímica, FACENA, Universidad Nacional del Nordeste, Campus Universitario, Corrientes, Argentina [b] INIFTA, Theoretical Chemistry Division, Buenos Aires, Argentina [c] CEQUINOR, Department of Chemistry, Faculty of Exact Sciences and Engineering Faculty, Buenos Aires, Argentina

To cite this Article Romero, J. M. , Profeta, M. I. , Jorge, N. L. , Gómez-Vara, M. E. , Castro, E. A. and Jubert, A. H.(2005) 'Structural and spectroscopic study of 3,6-dibutanoic-1,2,4,5-tetroxane', Molecular Simulation, 31: 14, 1075 — 1081
To link to this Article: DOI: 10.1080/08927020500271250
URL: http://dx.doi.org/10.1080/08927020500271250

Molecular Simulation, Vol. 31, No. 14–15, 15–30 December 2005, 1075–1081

Taylor & Francis
Taylor & Francis Group

Structural and spectroscopic study of 3,6-dibutanoic-1,2,4, 5-tetroxane

J. M. ROMERO†, M. I. PROFETA†, N. L. JORGE†, M. E. GÓMEZ-VARA†, E. A. CASTRO‡* and A. H. JUBERT¶

†Área de Fisicoquímica, FACENA, Universidad Nacional del Nordeste, Campus Universitario, Avda. Libertad 5400, 3400 Corrientes, Argentina
‡INIFTA, Theoretical Chemistry Division, Suc.4, C.C. 16, La Plata 1900, Buenos Aires, Argentina
§CEQUINOR, Department of Chemistry, Faculty of Exact Sciences and Engineering Faculty, C.C. 16, La Plata 1900, Buenos Aires, Argentina

(Received June 2005; in final form July 2005)

This paper deals with the synthesis of 3,6-dibutanoic-1,2,4,5-tetroxane and the theoretical study of its IR and UV spectra as well as the determination of its optimized molecular structure. Theoretical calculations are performed at the molecular dynamics (MD), molecular mechanics, semi empirical, *ab initio* and density functional theory (DFT) levels. The different structural and electronic effects determining the molecular stability of the conformers are discussed in a comparative fashion.

Keywords: Molecular dynamics; UV spectra; Density functional theory levels; Chemotherapy

1. Introduction

Malaria is one of the most deadly diseases affecting millions of people especially in developing countries [1–3]. The prevention and cure of malaria depend on a limited number of drugs. Apart from the natural product quinine, the synthetic drugs are quinoline derivatives, such as primaquine, chloroquine and mefloquine. Unfortunately, these traditional remedies are no longer adequate. The incidence of malaria by *Plasmodium Falciparum*, the most dangerous species of parasite, continues to grow steadily in many countries. Despite these alarming trends, we must point out the discovery that two naturally occurring peroxides, artemisinin and yinghaosu, possess potent antimalarial activity [4–6], so it is expected that suitable experimental developments of their derivatives will be capable of making important contributions in this field.

Rational design of structurally simpler analogs of artimisinin has led to synthesis of various trioxanes, some of which have excellent antimalarial activity [4–8]. EN LOS Last years there has been significant contributions to start a new chapter in the chemotherapy of malarial through the synthesis of new molecules having two endoperoxide groups, the 1,2,4,5-tetroxanes [9–11]. The tetroxanes represent a new class of potent, inexpensive peroxide antimalarial agents, which can be synthetized in a rather simple one step process starting from inexpensive materials.

This paper deals with the synthesis of 3,6-dibutanoic-1,2,4,5-tetroxane and its experimental and theoretical study of the IR and UV spectra. Theoretical calculations are performed at the molecular dynamics (MD), molecular mechanics, *ab initio* and density functional theory (DFT) levels. The different structural and electronic effects determining the molecular stability of the conformers are discussed in a comparative fashion.

2. Experimental section

2.1 Synthesis of glutaraldehyde acid diperoxide (GADP)

GADP (figure 1) is synthesized by oxidation of glutaraldehyde with oxygen peroxide in the presence of concentrated sulfuric acid, following the Bayer and Viller method modified by Jorge *et al.* [12].

A measured quantity of 68% H_2O_2 (0.04 mol, 1.36 g) and glutaraldehyde (0.0762 mmol, 7.62 g) were added by consecutive dropwise addition to a stirred solution of water (12 ml), EtOH (12 ml) and H_2SO_4 (12 ml) at -10°C. Stirring was continued for 4 h at -10°C. The resulting white precipitate was filtered, washed with water and air-dried. The precipitate was recrystallized in methanol.

*Corresponding author. Email: castro@quimica.unlp.edu.ar/direccion@inifta.unlp.edu.ar

Molecular Simulation
ISSN 0892-7022 print/ISSN 1029-0435 online © 2005 Taylor & Francis
http://www.tandf.co.uk/journals
DOI: 10.1080/08927020500271250

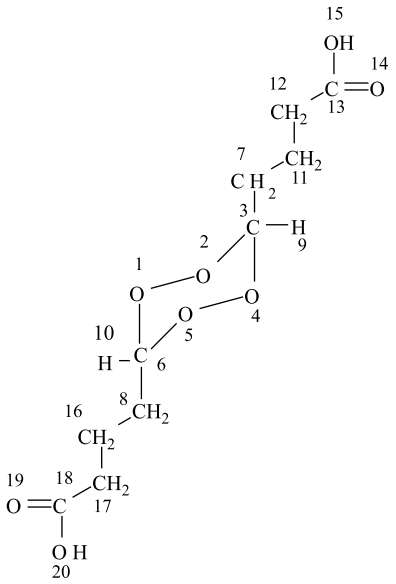

Figure 1. Glutaraldehyde acid diperoxide molecule.

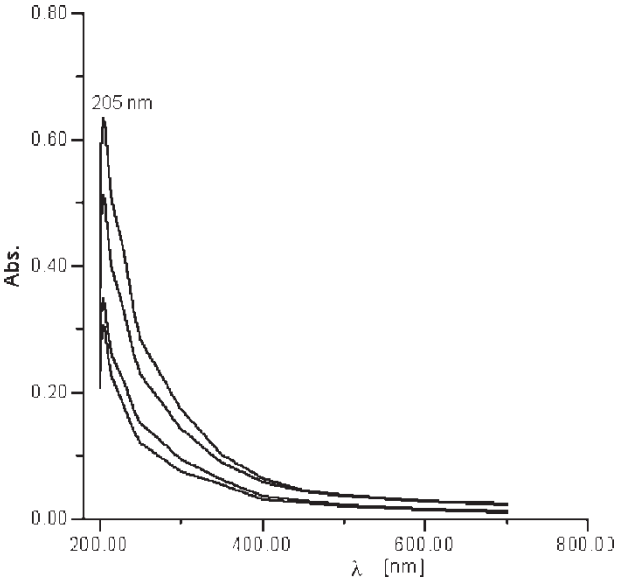

Figure 2. UV–visible spectrum obtained experimentally for the GADP.

The final product was obtained as a 1:1:2 mixture of stereoisomers.

Melting points were determined with a electrothermal capillary melting piont apparatus. The resulting values were of 63, 83 and 90°C, respectively, for each stereoisomer.

2.2 General

The synthesized DPAG was analyzed via UV and IR spectroscopic techniques. The UV visible spectrum was carried out in the 200–700 nm range (the quartz cell was 1 cm long, in a 0–2 absorbance range), in a trademark Camspec model M330 spectrophotometer. Standard solutions were employed. Infrared absorption spectra at room temperature from 1 cm diameter pellets made of the compound dilluted in spectrscopic grade KB were recorded on a IR Nicolet infrared spectrometer using the diffuse reflectance technique, between 400–4000 cm^{-1}.

3. Results and discussion

We obtained a white precipitate from the synthesis procedure. It was filtered, washed with water and dried at room temperature. The solid product was obtained in a 80% yield. The solid obtained is insoluble in water.

Figure 2 shows the UV–visible spectrum obtained experimentally for the GADP. Experimental spectrum within the studied wavenumber range presents only a peak at 205 nm. By comparison with reported values found in the literature [13] this band may be assigned to the peroxidic group O–O, due to the $\pi \rightarrow \pi^*$ electronic transition. We can assess this assignment since the dilution of the solutions does not change the position of the maximum of the absorption peak but only decreases its absorbance value.

In figure 3, we display the IR spectrum obtained experimentally for the GADP. It is interesting to note in this spectrum the presence of an absorption peak corresponding to the peroxidic O–O bond, which is characteristic for this sort of compound.

4. Computational methods

The conformational space for the molecule of the DPGA was studied using the MD module of the HyperChem package.[§] Several simulations were accomplished with the aid of the MM + force field which is also available in this package. The starting geometries were those characterized by the gauche, *cis*- and *trans*- conformations around the NH or C=O atoms between two rings. The starting geometries were heated from 0 to 600 K in 0.1 ps. Then, the temperature was kept constant by coupling the system to a simulated thermal bath with a bath relaxation time of 0.5 ps. The simulation time step was 0.5 fs. After an equilibration period of 1 ps a 500 ps-long simulation was run saving the coordinates every 1 ps. Those geometries were then optimized to an energy gradient less than 0.001 kcal mol^{-1} $Å^{-1}$ using the MM+ force field.

The energy conformers of the molecule were selected against energy intervals of 1 kcal between the highest and the lowest values of the collection and their selected geometries were optimized by means of the MNDO module of the HyperChem computational package.[§] Within a range of 7.65 kcal we found six conformers (see figures 4a–f). The conformer corresponding to the lowest energy (figure 4a) obtained according to the above methodology was further studied using the DFT theory as implemented in the Gaussian 98 package [14]. Geometry optimizations were performed using the Becke's three parameter hybrid functional [15,16],

[§]HyperChem Release 5.0 for Windows 1996, Hypercube Inc.,USA.

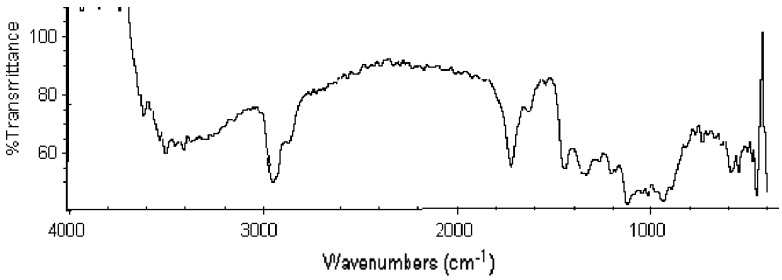

Figure 3. IR spectrum obtained experimentally for the GADP.

a combination that gives rise to the well known B3LYP method. The 6–31** G basis set is used for all the atoms. The Calculation with MNDO is subject to some criticism due to relatively poor description of the O–O bond.

In order to study the UV spectrum, we have employed the HyperChem package. The UV electronic spectrum was calculated at the most stable structure derived from the DFT theory at the semiempirical ZINDO/S method level through a single point calculation. The spectrum calculated via semiempirical ZINDO/S method is coincident with the experimental spectrum: where a single band with a maximum at 204.3 nm is found.

The vibrational spectra of the minimum energy conformer of the molecule was then calculated resorting to the DFT theory available in the Gaussian 98 package [14] using the same basis sets as above. The vibrational modes were assigned by means of their direct visualization with the help of the Molekel program [17].

In table 1, the geometrical optimized parameters of the different conformers calculated at Hartree-Fock level are collected together with those of the lowest energy conformer calculated at B3LYP/6–31G** level.

The stability order of the different conformers is analyzed taking into account four main factors considered in previous similar studies [18,19], plus two additional stereoelectronic effects and intramolecular interactions (hydrogen bond):

(a) Interaction among adjacent free electron pairs [20,21], located on the oxygen atoms. Assuming a tetrahedral hybridization for the oxygen atom located at the ring, repulsion between free electron pairs is lower in the twist conformations than the chair conformation. In this effect, the repulsion between two electron is considered to decrease in the following order: free-pair-free-pair $>$ free-pair-σ $>$ σ-σ, and it reveals itself through anomalous bond angles, with deviations of lineal three center bonds which are usually attributable to free-electron pairs-σ repulsions.
(b) The torsion angle around the O–O bond favors the twist form since this is the less distorted conformation. Results are presented in table 1.
(c) Sterical effect, according to the location of the butyric group at the equatorial or axial positions [19].

Table 1. Calculated and experimental geometric parameters of glutaraldehyde acid diperoxide molecule.

	Conformers				
	RHF 3-21+G	*RHF 6-31G*	*RHF 6-311G*	*B3LYP 6-31** G*	*Exp.*
Bond length (Å)					
O_1O_2	1.464	1.454	1.436	1.462	1.480
C_3O_2	1.453	1.436	1.436	1.418	1.410
C_3O_4	1.454	1.438	1.434	1.422	1.430
C_3C_7	1.517	1.513	1.512	1.522	1.520
C_7C_{11}	1.538	1.533	1.532	1.547	1.523
$C_{11}C_{12}$	1.533	1.529	1.527	1.552	1.531
$C_{13}C_{12}$	1.500	1.497	1.494	1.509	1.524
Bond angle (degrees)					
$C_3O_4O_5$	107.98	108.64	108.96	106.47	107.60
$O_2C_3O_4$	106.63	107.08	107.15	106.47	106.90
$O_1O_2C_3$	107.30	108.31	108.59	106.06	107.10
$C_7C_3H_9$	114.20	113.66	113.46	113.82	112.70
$O_2C_3C_7$	113.69	114.04	113.96	112.91	113.20
$O_4C_3C_7$	113.23	113.12	113.14	114.33	112.30
$C_3C_7C_{11}$	112.89	113.90	114.00	112.88	111.60
$C_7C_{11}C_{12}$	112.90	113.75	113.89	113.10	111.50
$C_{11}C_{12}C_{13}$	112.20	112.83	112.98	111.57	111.40
Torsion angle (degrees)					
$C_6–O_1–O_2–C_3$	64.40	63.68	63.18	63.79	
$C_6–O_5–O_4–C_3$	−66.61	−64.55	−64.22	−63.17	
$O_4–C_3–O_2–O_1$	65.16	63.28	62.79	65.82	
$O_5–O_4–C_3–O_2$	−64.12	−62.83	−62.25	65.40	

(d) Anomeric effect of the endocyclic oxygen free electron pairs exert on the endo C–O bond and on exo C–C bonds, when the butyric group is located at the axial position.
(e) Exoanomeric effect that free electron pairs of the oxygen atom belonging to the substituent group exert on the C–Oendo bond in the synclinal and antiperiplanar conformations.
(f) Stabilizing interaction by means of intramolecular hydrogen bonds, which stabilizes a conformer with respect to the other due to the existence of a bonding interaction involving the hydrogen atom of the substituent with the oxygen atom located at the ring.

The synclinal conformer with two anomeric effects and another exanomeric effect is the most stable one. The Hartree Fock method with the 6-31G and 6-311G basis sets shows a shortening of the C–Cexo bond, which reveals the stereoelectronic interactions. This effect is more pronounced in the minimum energy structure computed via the B3LYP method with the 6-31G** basis set (table 1).

The Hartree Fock method with 6-31G and 6-311G basis sets describes quite satisfactorily the bond length variations of the C–Oendo and C–Cexo bonds for these compounds. Results derived from the B3LYP method with the 6–31**G basis set are quite close to the experimental data (table 1).

Assuming a tetrahedral hybridization for the oxygen atom, the repulsions between the 1,5 syn-axial electron lone pairs are smaller in the twist conformer than in the chair one. This feature may be rationalized on the basis that electron lone pair moment are less parallel in the first conformer than in the second one. The effect is magnified with the decrease of the OCO bond angle and the increasing of the HCC bond angle (table 1). This particular effect contributes to the stabilization of the twist geometry.

The interaction between electron lone pairs in adjacent oxygen atom in the ring, contributes to the stabilization of the chair geometry.

The syn-axial effect and the torsion angle factor play an important role in order to determinate the stability of the twist structure.

The 1,2 interaction of electron lone pair between oxygen atoms, the sterical effect, the anomeric effect, the exoanomeric effect and the intramolecular interaction (hydrogen bonds) contribute to the stabilization of the chair geometry.

In table 2, we present both experimental and theoretical IR spectra as well as the corresponding assignement of the different vibrational modes of the molecule under study.

In solid state GADP displays bands at 3523 and 3539 cm^{-1} (calculated data are 3530 and 3531 cm^{-1}, respectively), which are assigned as the stretching modes $\nu O_{11}H_{33}$ and $\nu O_{18}H_{34}$, respectively.

The band at 2754 cm^{-1} is assigned to a symmetrical CH_2 stretching mode and theoretically these bands are calculated at 2811 and 2845 cm^{-1} while the asymmetrical CH_2 stretching bands are located at 2871, 2872, 2943 and 2947 cm^{-1} and they are calculated at 2867 and 2918 cm^{-1}.

The C=O groups absorb at 1630(sh) and 1722 cm^{-1} and the corresponding calculated values are 1744 and 1745 cm^{-1}. These bands are assigned to the *cis* and *trans* conformers, respectively. The bands at 1120 and 1118 cm^{-1}, calculated at 1121 and 1112 cm^{-1}, respectively, correspond to coupled modes among νC=O, νCN, νCC, rocking and twisting CH_2.

Bands calculated between 1212–1506 cm^{-1} correspond to different CH_2 bend, wag, rock and twisting modes. Experimental bands at 1443–1445, 1350, 1344, 1331, 1273, 1268, 1208–1205 cm^{-1}, calculated at 1422, 1358, 1343, 1331, 1289, 1263, 1212 cm^{-1}, respectively, are assigned as CH_2 wagging and CH bending; twist and wag CH_2, δOCO, νCC and CH bending; CH bending and CH_2 twist; CH bend, wag and rocking CH_2; wag and twist CH_2, δCC, δCOH and OH wagging; twisting CH_2, CH bend, νCO and OH wagging; twisting CH2 and CH bend, respectively

Bands calculated between 967 and 1121 cm^{-1} are highly coupled among different movements as described in the table.

The C–O stretching bands calculated at 1160 and 1169 cm^{-1} are correlated with the peaks at 1118 and 1182 cm^{-1}.

The OCO deformation mode at 1053 cm^{-1} is coupled with twist, wag and rocking CH_2 modes and calculated at 1054 cm^{-1}.

Bands at 1004, 1018–1049 cm^{-1} correspond to C–O and C–C stretching modes and their calculated values correspond to 994 and 1039 cm^{-1}, respectively.

The corresponding O–O stretching modes of the ring are located at 934–936 cm^{-1} and calculated at 913, 946, 962 cm^{-1} as single modes, while the bands at 909 and 893 cm^{-1} correspond to the asymmetric and symmetric O–O coupled stretching modes.

The bands at 816–818, 702–735 and 599, 670 and 637 cm^{-1}, calculated at 822, 729 and 600 cm^{-1}, 656–630 cm^{-1}, respectively, are assigned as COO deformation modes, asymmetric and symmetric O_4 ring deformation and OCO deformation modes, respectively.

Bands located between 585 and 412 cm^{-1} and calculated between 586 and 428 cm^{-1} correspond to torsion angles coupled with wag, rock and twisting CH_2 modes.

5. Conclusions

The main conclusions derived from this joint experimental and theoretical study of DPAG are the following:

– The technique employed for this tetroxane derivative is inexpensive and rather simple and it allows one to obtain a solid with a high yield (80%).
– Absorption at 205 nm in the UV spectrum can be assigned to the O–O group. There is a satisfactory agreement with the calculated value at the ZINDO semi empirical level of calculation.
– A complete assignment of the vibrational IR spectrum was presented and a comparison between theoretical and experimental spectra was made.

Table 2. Experimental, theoretical B3LYP vibrational frequencies and assignment of 1,3- dibutanoic-1,2,4,5-tetroxane.

Calcutated B3LYP vibrational frequencies	*Experimental vibrational frequencies*	*Assignment*
17		τC4C13C14H22, τH19C13C14H21, τH20C13C14H21
22		τO11C10C9H26, τH33O12C10C11
31		τC7C1O6O5, τO2O3C4O5
34		τO17C16O18H34
50		τH31C1O2O3, τO6O5C4O3, τO17C16O18H34
51		τH31C1O6O5, τO6C1O2O3, rocking C15H23,24, νC16O17
83		τH20C13C14H22, rocking C9,14,15H25-26, 21-22, 23-24
97		τH26C9C8H30
104		τH26C9C8H29, τH19C13C14H22, τO17C16C15C14
158		τH21C14C13H19, rocking C8H29-30
164		τH33O12C10O11, τC9C8C7H27, τH19C13C14H22
214		τH29C8C7H28, τH20C13C4O3, rocking C8H29-30
224		τH23C15C14H22, rocking C15,14H23-24, 21-22
251		τH30C8C7H28, rocking C8;13,14,15H29-30; H19-24, H21-22, H23-24
269		τC7C1O2O3, τO3C4C13H19, τO17C16C15H23
299		τH31C1O2O3, τH31C1O6O5, τO6O5C4H32, τO2O3C4O5
314		τH28C7C1H31, τH31C1O6O5, wag C7H27-28
355		τH32C4C13H19, τO5C4C13H20, rocking C15H23-24
428	412	τC9C8C7H27, τO11C10C9C8, rocking C7H27-28
	423	
456		Wagging O18H34, rocking C15H23-24
457	454	τH34O18C16C15, τH33O12C10O11
467		τH33O12C10C9, rocking C9H25-26, δC10O12H33, νC10O12
477	478	τC8C7C1O6, τC8C7C1H31, τC9C8C7C1, rocking C8H29-30
	482	
504	504	τH34O18C16C15, τO3C4O5O6, τH31C1O2O3
527		τH31C1O6O5, τC8C7C1H31, rocking C7,8H27-28, 29-30, bend C4H32, rocking C13,14H19-20, 21-22
559	548	τO17C16O18H34, rocking C15H23-24
	557	
575		τH33O12C10O11, τO12C10C9H25, rocking C9H25-26
586	585	τH24C15C16O18, νO5C4, wag C4H32, wag C13H19-20, τH34O18C16C15, rocking C15H23-24, δO17C16O18
600	599	Sym ring def. O2,3,5,6
630	637	δO17C16O18, rocking C13,14,15H19-20,21-22,23-24, νC16O18
656	670	δO11C10O12, rocking C7,9H27-28,25-26, δC10C9C8
729	702–707	Asym ring def. O2,6 ↓ O3,5 ↑ , rocking C7,9H27-28,25-26, bending C4H32
	733	
	735	
770	771	Rocking C13,14H19-20, 21–22
789		Rocking C8,9H29-30, 25-26
822	816	δC1O6O5, bend C1H31, rocking C7,8,9H27-28,29-30,25-26
	818	
836		δC4O3O2, bending C1H31, rocking C13,14H19-20,21-22
881		δO2O3C4, rocking C13,14,15H19-20,21-22,23-24, νO6O5, νC1O2
893	896	Sym νO2O3, νO5O6, twist C7H27-28, rocking C8,9H29-30,25-26, νC10O12, νC10O11
909		Asym νO5O6, νO2O3, twist C7H27-28, rocking C8,9H29-30,25-26, νC10O12, νC10O11
913		νO5O6, δC1O2O3, twist C13H19-20, rocking C14,15H21-22,23-24
946	934	νO2O3, ring def., twist C13H19-20, rocking C14,15H21-22,23-24
	936	
962		νO5C4, νC1O6, δC7C1O2, wagging C7H27-28, rocking C8,9H29-30, 25-26
967		Twist C7,8H27-28,29-30, wag C9H25-26, bend C1H31, δO6C1O2
994	1004	νC4O5, ring def., rocking C15,14H23-24,21-22, wag C15H23-24
1039	1018	νC1O2, νC7C8, wag C8,9H29-30, 25-26, rocking C7H27-28
	1049	
1054	1053	δO3C4O5, twist C13H19-20, wag C14H21-22, rocking C15H23-24
1077		Wag C13,14H19-20,21-22, νC13C14, bend C1H31, rocking C7H27-28, νC1C7
1085		Wag C13,14H19-20,21-22, bending C1,4H31,32, νC13C14, wag C13,14H19-20,21-22, rocking C7,8H27-28, 29-30
1096		νC7C8, νC8C9, δH32C4C13, wag C13H19-20, rocking C7,8,9HH27-28,29-30,25-26, νC4O3
1109		νC14C15, rocking C8,9,13,14,15HH29-30H25-26, H19-20,H21-22,H23-24, wag O18H34
1112	1118	νC4C3, bend C4H32, νC14N15, rocking C13H19-20, νC16O17
1121	1120	νC10C9, νC9C8,, νC10O11, twist C9H25-26, bend C8,7,1 H29,27,31
1160		νC10O12, wag O12H33, wag C9H25-26, δC9O10O11, wag O18H34
1169	1182	νC16O18, wag O12H33, wag C15H23-24, δC13H19-20
1212	1205	Twist C8H29-30, twist C9H25-26, bend C7H28
	1208	
1220		Twist C13H19-20, bend C14H22, twist C15H23-24, δC13C4O3
1259		Bend C13,14,15H19,21,24, δO5C4H32
1263	1268	Twist C7H27-28, bend C8,1H30,31, νC1O6, wag O12H33
1289	1273	Wag C9H25-26, twist C7H27-28, δC7C8C9, δC10O12H33, wag O12H33

Table 2 – *continued*

Calcutated B3LYP vibrational frequencies	*Experimental vibrational frequencies*	*Assignment*
1291		Wag C15H23-24, bend C4,13,14H32,19,21, twist C7H27-28, δO17C16O18
1314		bend C4,13,14H32,20,21, twist C15H23-24
1323		Bend C1H31, wag C7H27-28, twist C8,9H29-30, 25-26
1331	1331	Bend C4,15H32,24, wag C15H23-24, rocking C14H21-22
1345	1344	Bend C1,7,8,9H31,27,30,25, twist C9H25-26
1358	1350	Twist C7H27-28, bend C8,9H29,26, δO11C10O12, wag C9,8H25-26,29-30, νC9C10
1376		Bend C1,4H31,32
1383		Bend C1,4, 7,13H31,32,28,9, wag C14H21-22, νC13C4
1392		Bend C1,4H31,32, twist C13,7H19-20,27-28
1402		Twist C14H21-22, wag C15H23-24, δC16C15H23
1409		Bend C1H31, wag C7H27-28, twist C8H29-30, twist C13H19-20, wag C14H21-22
1419		Wag C13,14H19-20,21-22, bend C4H32, wag C8,9H29-30,25-26, twist C7H27-28
1422	1443	Wag C7,9,13,14H27-28,25-26,19-20,21-22, bend C1,4H31,32
	1445	
1475		δH23C15H24
1483		δH25C9H26
1490		δH27C7H28
1494		δH21C14H22, δH19C13H20 (in phase)
1505		δH29C8H30
1506		δH19C13H20, δH21C14H22 (out of phase)
1744	1630sh	νC16O17, δC16O18H34
	1722	
1745		νC10O11, δC10O12H33
2811	2754	Sym νC15H23,24, sym νC9H25,26
2818		Sym νC14H21,22
2838		Sym νC13H19,20, νC14H21, νC4H32
2844		Sym νC7H27,28
2845		νC4H32, sym νC13H19,20
2847		Asym C15H23,24, sym νC14H21,22, νC4H32
2852		Sym νC8H29,30
2856		νC1H31, sym νC8H29,30
2867	2871	Asym νC9H25,26, asym νC8H29,30
	2872	
2890		Asym νC7H27,28, asym νC8H29,30
2897		Asym νC8H29,30, asym νC7H27,28
2900		Asym νC14H21,22, asym C13H19,20
2918	2943	Asym νC13H19,20, asym νC14H21,22
	2947	
3530	3523	νH33O11
3531	3539	νH34O18

We have performed a conformational study of DPAG with the MNDO method and it predicts the chair structure to be the most stable one.

– The assignment of the O–O stretching mode corresponding to the IR spectrum can be done unambiguously by means of theoretical *ab initio* calculations and it corresponds to the band found within the range 943–936 cm^{-1} calculated at 913, 946, 962 cm^{-1}, respectively.

Acknowledgements

Authors thank warmly several valuable referees' comments, which have been helpful to get an improved final version of this article. AHJ is member of the Research Career of CIC, PBA, Argentina.

References

[1] L.J. Bruce-Chwatt. *Chemotherapy of Malaria*, 2nd ed., p. 104, WHO, Geneva (1981), Chapter 5.

[2] D.J. Wyler. Malaria-resurgence, resistence and research. *N. Engl. J. Med.*, **308**, 875 (1983); *ibid* 934–940.

[3] C. Hansch, A. Leo. Exploring QSAR. *Fundamentals and Applications in Chemistry and Biology*, ACS Professional Reference Book, American Chemical Society, Washington, DC, 1995, p.442.

[4] W.S. Zhou, X.X. Xu. Total synthesis of the antimalarial sesquiterpene peroxide qinghaosu and yingzhaosu A. *Acc. Chem. Res.*, **27**, 211 (1994).

[5] R.K. Haynes, S.C. Vonwiller. From quinghao, marvelous herb of antiquity, to the antimalarial trioxane qinghaosu- and some remarkable new chemistry. *Acc. Chem. Res.*, **30**, 73 (1997).

[6] J.N. Cumming, P. Ploypradith, G.H. Posner. Antimalarial activity of artemisinin (qinghaosu) and related trioxanes: mechanism of action. *Adv. Pharmcol.*, **37**, 253 (1997).

[7] C.W. Jeffort, J. Velarde, G. Bernardelli. Synthesis of tricyclic Artemisinin-like compounds. *Tetrahedron Lett.*, **30**, 4485 (1989).

[8] C.W. Jeffort, S.J. Jin, G. Bernardelli. Reactions of an endoperoxides with chiral ketones. Diastereoselective formation of 1,2,4-trioxanes and 1,3-dioxolane. *Tetrahedron Lett.*, **32**, 7243 (1991).

[9] J.L. Vennerstrom, F. Hong-Ning, W.Y. Ellis, A.L. Ager, Jr., J.K. Wood, S.L. Andersen, L. Gerena, W. K. Milhous. Dispiro-1,2,4,5-tetroxanes: a new class of antimalarial peroxides. *J. Med. Chem.*, **35**, 3023 (1992).

[10] J.L. Vennerstrom, Y. Dong, S.L. Andersen, A.L. Ager, Jr., H-N. Fu, R.E. Miller, D.L. Wesche, D. Kyle, L. Gerena, S.M. Walters, J.K. Wood, G. Edwards, A.D. Holme, W.G. Maclean, W.K. Milhous. Synthesis and antimalarial activity of 16 dispiro-1,2,4,5-tetraoxanes: alkyl-substituted 7,8,15,16-tetraoxadispiro[5.2.5.2]hexadecanes. *J. Med. Chem.*, **43**, 2753 (2000).

[11] J.L. Vennerstrom, A.L. Ager, Jr., S.L. Andersen, L.G. Steven, M. James, V. Wongpanich, C. Angerhofer, J.K. Hu, D.L. Wesche.

Assessment of the antimalarial potential of tetraoxane WR 148999. *Am. J. Trop. Med. Hyg.*, **62**, 573 (2001).

[12] L.C.A. Leiva, J.M. Romero, N.L. Jorge, M.E. Gómez Vara. Síntesis y descomposición térmica del diperóxido de formaldehído. *Rev. Int. Inf. Tecnol.*, **13**, 0716 (2002).

[13] L.C.A. Leiva, J.M. Romero, N.L. Jorge, M.E. Gómez Vara, E.A. Castro. UV and IR spectroscopic study of the 1,2,4,5-tetroxane. A joint experimental and theoretical analysis. *Asian J. Spect.*, **5**, 177 (2001).

[14] Gaussian 98, Revision A.7, M.J. Frisch, G.W. Trucks, H.B. Schlegel, G.E. Scuseria, M.A. Robb, J.R. Cheeseman, V.G. Zakrzewski, J.A. Montgomery, Jr., R.E. Stratmann, J.C. Burant, S. Dapprich, J.M. Millam, A.D. Daniels, K.N. Kudin, M.C. Strain, O. Farkas, J. Tomasi, V. Barone, M. Cossi, R. Cammi, B. Mennucci, C. Pomelli, C. Adamo, S. Clifford, J. Ochterski, G.A. Petersson, P.Y. Ayala, Q. Cui, K. Morokuma, D.K. Malick, A.D. Rabuck, K. Raghavachari, J.B. Foresman, J. Cioslowski, J.V. Ortiz, A.G. Baboul, B.B. Stefanov, G. Liu, A. Liashenko, P. Piskorz, I. Komaromi, R. Gomperts, R.L. Martin, D.J. Fox, T. Keith, M.A. Al-Laham, C.Y. Peng, A. Nanayakkara, C. González, M. Challacombe, P.M.W. Gill, B. Johnson, W. Chen, M.W. Wong, J.L. Andrés, C. González, M. Head-Gordon, E.S. Replogle, J.A., Pople, Gaussian, Inc., Pittsburgh PA (1998).

[15] A. D. Becke. Density-functional thermochemistry. III—The role of exact exchange. *J. Chem. Phys.*, **98**, 5648 (1993).

[16] C. Lee, W. Yang, R.G. Parr. Development of the Colle-Salvetti correlation energy formula into a functional of the electron density with the Lee–Yang–Parr correlation functional. *Phys. Rev. B*, **37**, 785 (1988).

[17] MOLEKEL 4.0, P. Flúkiger, H.P. Lúthi, S. Portmann, J. Weber, Swiss Center for Scientific Computing, Manno (Switzerland) (2000).

[18] N. Jorge, M. Gómez-Vara, L.F.R. Cafferata, E. A. Castro. Theoretical study of the trans 3,6-dimethoxy-1,2 dioxane molecule. CPS: orgchem/0101001 *Krag. J. Science*, **24**, 57 (2002).

[19] N.L. Jorge, E.A. Castro, J.C. Autino, L.R.F. Cafferata. Experimental and theoretical study of trans-3,6-diphenyl-1,2,4,5-tetroxane molecule. *J. Mol. Struct. Theochem.*, **459**, 29 (1999).

[20] A. Pinchas, A. Yitzhak, A. Ellencwieg, B. Fuchs, Y. Goldberg, M. Karni, E. Tartakovsky. Probing the anomeric effect. Trimethylsilyloxy and tert-butoxy substituents in the 1,4-dioxane derivatives: theory vs. experiment. *J. Am. Chem. Soc.*, **109**, 1486 (1987).

[21] O.G. Stradella, H. Villar, E.A. Castro. A theoretical conformational study of s-Tetrathiane, s-Tetroxane and their methyl derivatives. *J. Mol. Struct. Theochem.*, **135**, 7 (1986).